Title
Probing Cell Adhesion Profiles with a Microscale Adhesive Choice Assay

Journal
Biophysical Journal, 113(8)

ISSN
0006-3495

Authors
Kittur, Harsha
Tay, Andy
Hua, Avery
et al.

Publication Date
2017-10-01

DOI
10.1016/j.bpj.2017.08.028

Peer reviewed

Biophysical Journal
Article

Biophysical Society

Probing Cell Adhesion Profiles with a Microscale Adhesive Choice Assay

Harsha Kittur,[1] Andy Tay,[1] Avery Hua,[1] Min Yu,[2] and Dino Di Carlo[1,3,4,*]
[1]University of California Los Angeles, Los Angeles, California; [2]University of Southern California, Los Angeles, California; [3]California NanoSystems Institute, Los Angeles, California; and [4]Jonsson Comprehensive Cancer Center, Los Angeles, California

ABSTRACT In this work, we introduce, to our knowledge, a new set of adhesion-based biomarkers for characterizing mammalian cells. Mammalian cell adhesion to the extracellular matrix influences numerous physiological processes. Current in vitro methods to probe adhesion focus on adhesive force to a single surface, which can investigate only a subcomponent of the adhesive, motility, and polarization cues responsible for adhesion in the 3D tissue environment. Here, we demonstrate a method to quantify the transhesive properties of cells that relies on the microscale juxtaposition of two extracellular matrix-coated surfaces. By multiplexing this approach, we investigate the unique transhesive profiles for breast cancer cells that are adapted to colonize different metastatic sites. We find that malignant breast cancer cells readily transfer to new collagen I surfaces, and away from basement membrane proteins. Integrins and actin polymerization largely regulate this transfer. This tool can be readily adopted in cell biology and cancer research to uncover, to our knowledge, novel drivers of adhesion (or de-adhesion) and sort cell populations based on complex phenotypes with physiological relevance.

INTRODUCTION

Physical interactions of mammalian cells with their microenvironment influence numerous key cellular functions such as motility, growth, survival, and differentiation. In cancer, invasion and metastasis are likely underpinned by abnormal adhesive programs, which allow cells to colonize and spread along new extracellular matrix (ECM) compositions that differ from the original tissue structure, following the seed-to-soil hypothesis. In this hypothesis, tumor cell "seeds" settle in microenvironments with the most suitable "soil" (1–3) through favorable soluble and adhesive interactions.

In breast cancer patients, mortality is largely due to metastases from the primary tumor to secondary sites such as bone (4–6), lung (7), and brain (8,9) tissue, each with unique ECM (10). However, current tumor cell analysis often fails to predict propensity for metastasis. For a localized tumor, current prognostic markers are insufficient to confidently assess metastatic risk in 70% of all breast cancer patients (4). Secondary site prediction markers are especially in demand, furthering the need for new quantitative and high-throughput techniques to analyze biopsied cells. Molecular analysis tools have shed some light on the expression level changes of adhesion proteins for site-specific metastatic cells. For example, cells that metastasize to bone tend to overexpress the osteopontin gene (11), whereas those that metastasize to lung have increased expression of tenascin C (12).

These promising gene-expression signatures for breast tumors may be complemented with novel phenotypic biomarkers for a wide range of physical properties associated with metastasis (13) such as deformability (14,15), size (16), contractility (17), or adhesion (18). Identifying cells that adhere to microenvironments with specific morphology, forces, ECM type, and ECM density may be particularly useful for determining likely metastatic destinations in breast cancer (18).

Previous technologies to characterize cell adhesion have led to quantitative measures of adhesion strength (19)—measurements that encompass numerous other cellular-level parameters such as cell size, spread area, contractility, cell-cell contacts, and degradation rate of adhesive moieties. Many of these adhesion-based characterization tools rely on attaching cells to 2D surfaces on which they spread a varying amount, and then characterizing shear stress or other forces required to detach the cells. Therefore, the overall force of adhesion is dependent on the surface properties, geometry-dependent stresses, and active processes of cell spreading and surface degradation. These 2D surfaces also do not activate the dorsal ligands (20), and therefore do not represent the morphology and migration of cells in vivo (21) where cells receive chemical cues from all directions (21–23).

Submitted May 31, 2017, and accepted for publication August 15, 2017.
*Correspondence: dicarlo@seas.ucla.edu
Editor: Alexander Dunn.
http://dx.doi.org/10.1016/j.bpj.2017.08.028

Here we present a multiplexed transhesion platform that sandwiches cells between different ECM protein-coated surfaces to determine a relative adhesive signature. This format allows multidirectional exposure of cells to ECM, which, in comparison to 2D surfaces, can better model the 3D in vivo environment with the ECM degradation activity, cell motility, and cell adhesion that is involved in metastatic spread. We determined that cells with mesenchymal phenotype can transfer away from an originally seeded surface and adhere to a new surface, a process we term "transhesion". We find that transhesion is largely dictated through actin polymerization, integrin composition, and potentially ECM degradation. Using the same mechanisms, we demonstrate the ability to enrich cell subpopulations by their unique "transhesive" characteristics, which may enable subsequent physical or genetic characterization with increased signal-to-noise in the future (16,24).

MATERIALS AND METHODS

Experimental design

The objective of this study was to design a platform that measures cell transhesive potential, or the ability of cells to transfer their adhesion from one surface to another. Laser-cut acrylic pieces were designed around a standard 60-mm petri dish, and standard microfabrication protocols were performed to construct the surfaces. All conditions were tested at least in triplicate, although $n > 3$ for most experiments. This was largely dependent on satisfying the condition that the number of cells in each experiment's population must be >100, as indicated in Fig. S3, *a* and *b*. Any samples with $n < 100$ were not included in the data analysis. Protein stripes were randomized in Fig. 2, and were patterned in alternating types (e.g., C1, C4, Ln, C1, C4, Ln…) for the all other experiments to eliminate any bias from compression.

Photolithography

All wafer molds were developed using standard photolithography methods. New wafers were cleaned with acetone, methanol, and isopropanol. Molds for the glass substrates were created by spinning KMPR 1005 (MicroChem, Westborough, MA) at 5000 and 1000 RPM/s for 30 s to achieve the height of 5 μm. Molds for PDMS striping channels required KMPR 1050 (MicroChem) spun at 2000 and 1000 RPM/s for 30 s to achieve ~70 μm height. After soft-baking for 5–7 min, wafers were exposed to UV light for 30 s or 3 min, respectively, through a photomask. Due to the large features of the photomask, the mask was simply designed in Inkscape (https://inkscape.org) and printed on two transparencies with a standard laser printer. The transparencies were first taped together, and then they were taped against a 5" ± 5" glass. After exposure, wafers were hard-baked for 2 min before developing in MF-26A for at least 2 min to etch away unpolymerized photoresist. Wafers were baked for 2 min, and feature heights were confirmed using a reflectometer (NanoSpec; Nanometrics, Milpitas, CA) and profilometer (Dektak; Bruker, Billerica, MA). Finally, wafers were exposed to 10 min of HMDS coating to render the surfaces hydrophobic.

Glass substrate preparation

1.5" × 1.5" glass squares were cut with a glass cutter from 1.5" × 3" glass slides, and the corners were chipped off to allow the squares to fit comfortably in a 60-mm-diameter petri dish. Glass pieces were cleaned with ethanol or isopropanol and mechanical scrubbing. Scotch tape was applied to one side for protection. Laser-cut acrylic frames were clipped over the wafers to position glass pieces directly over the patterned regions of the wafer. A drop of PDMS was placed on each of the glass pieces, which were flipped and pressed against the stripe patterns (Fig. S1), resulting in a very thin layer (40–60 μm) of patterned PDMS. These treated glass pieces were allowed to partially cure at room temperature overnight, followed by full cross-linking in a 60°C oven. The slow partial cure step at room temperature prevents PDMS expansion against the features of the wafer, which facilitates removal. After unclipping the acrylic alignment frames, the glass substrates were removed gently with a razor blade.

PDMS striping channel layer fabrication

PDMS protein striping channels were made using a standard PDMS molding process. Aluminum foil walls were created to contain liquid PDMS. Approximately 25–30 g of PDMS was poured onto the wafer, and this was degassed in a vacuum chamber for 30 min. The PDMS was then cured in a 60°C oven overnight, and it was peeled away from the wafer. The PDMS was cut around the stripe patterns (channels) using a razor blade, and holes were punched for the inlet and outlet of each channel.

Protein coating

The tape on the back of the PDMS-glass pieces was removed, and each substrate was cleaned from dust with tape and isopropanol. A solvent of 95% ethanol and 5% water in a beaker was prepared. To this, 1% glacial acetic acid and 1% 3-aminopropyltriethoxysilane were added, and a magnetic stir bar was used to vigorously mix the solution for 15 min. During this time, PDMS-glass pieces were exposed to air plasma (Harrick Plasma, Ithaca, NY) for 1 min at 500 mTorr. These surfaces were immediately submerged in the 3-aminopropyltriethoxysilane mixture, and the reaction was set to shake gently on a stir plate for 45 min. This rendered the surfaces positively charged, and thereby enabled electrostatic binding of the negatively charged proteins at pH 7.

Protein solutions were simultaneously formulated at 100 μg/mL concentrations. Eight different ECM proteins were patterned (Fig. S2 *b*), including the glycoproteins fibronectin (Fn; Invitrogen, Carlsbad, CA) and fibrinogen (Fg; Sigma-Aldrich, St. Louis, MO); the abundant fibrillar protein collagen I (C1; Sigma-Aldrich); basement membrane proteins like collagen IV (C4) and laminin (Ln; Invitrogen); the invasion-mediating protein vitronectin (Vn; Advanced Biomatrix, Carlsbad, CA) (25); the lung invasion-mediating protein tenascin C (Tn; EMD Millipore, Billerica, MA) (12); and the bone invasion-mediating protein osteopontin (On; R&D Systems, Minneapolis, MN) (11).

After preparing protein solutions, PDMS-glass substrates were washed twice with reagent-grade ethanol, air dried, and placed in a fresh petri dish. Each PDMS striping channel was overlaid on a PDMS-glass substrate, and a benchtop magnifying glass was used to align the striping channels with the stripes on the glass. Eight microliters of protein solution was injected into each inlet according to the predetermined arrangement of proteins, and was let to sit for 1 h at room temperature. Finally, remaining solutions were extracted from each inlet, and the protein-striped glass substrates were left to dry overnight at room temperature.

Cell culture

All MDA-MB-231 cell lines, including variants TGL/1833, TGL/4175, and TGL/Brm-2a, were cultured in DMEM with 10% FBS and 1% Penn/Strep. Molecular-level characterization of these organ-tropic cell lines are described elsewhere (6–9). The human mammary epithelial cells (hMECs) line was cultured using the MEGM BulletKit (Lonza, Basel, Switzerland).

Upon confluency of ~80%, cells were passaged following traditional techniques. Cells were treated with 0.05% trypsin to detach them from the culture surface, and then centrifuged at 1400 RPM. Passage number ranged from 5 to 30.

Multiplexed cell adhesion assay

All proteins were tested in parallel in the multiplexed format of the assay, in which proteins were patterned in stripes along the 5-μm-deep trenches. Upon compression, this format exposed cells to 64 combinations of ECM protein pairs at once for rapid analysis and improved experimental control (Fig. 1 *d*). Stripe cross regions are identified as the regions of interest (ROIs) (Fig. S2 *c*). Cells were labeled with Hoechst 33342 nuclear stain, and upon separation they were enumerated to determine their transfer rate in the selected ROIs. A heat map for each cell population with respect to each protein pair was developed to characterize its relative adhesive landscape, where darker orange indicates greater transfer to the top surface and darker blue indicates proclivity to the bottom surface.

Cell compression

Before cell passaging, all surfaces were sterilized in the biosafety cabinet under 15 min of UV exposure. One milliliter of cells was passaged and passed through a 40-μm-pore-size filter to remove cell aggregates before seeding onto the protein-striped substrates at 500,000 cells/mL. Cells were placed in an incubator at 37°C and 5% CO_2 for 2 h to adhere to the bottom surface. After this time, cells were washed and stained with calcein AM and Hoechst 33342 to stain for live cells and the nucleus, respectively.

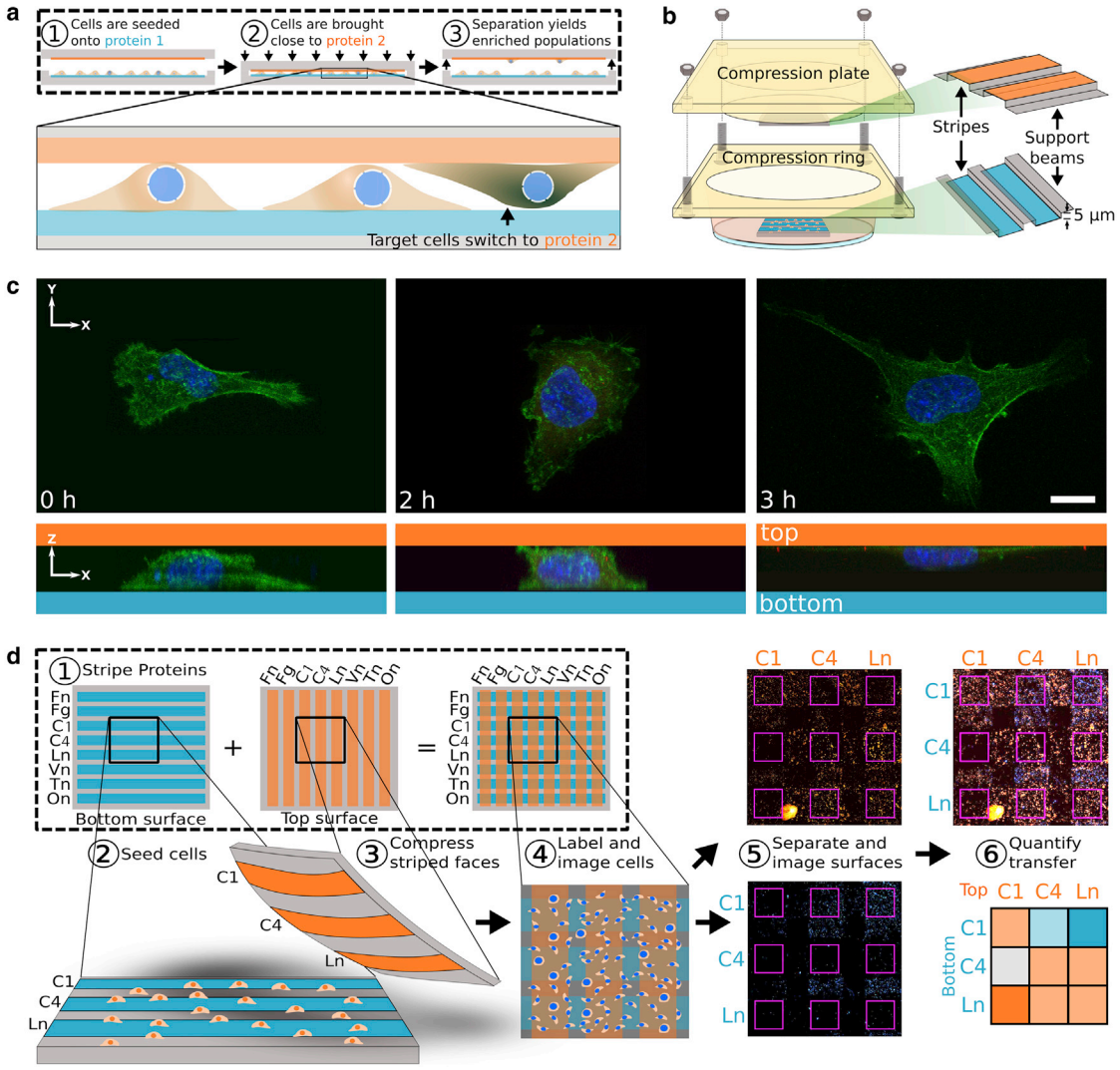

FIGURE 1 Transhesion concept and workflow. (*a*) A cell population is being exposed to two different protein-coated surfaces, by which some cells choose to transfer to the top surface, where they remain upon separation. (*b*) The transhesion platform is constructed around a standard 60-mm-diameter petri dish. Proteins are coated in the PDMS micropatterned trenches, and the two surfaces are compressed such that trenches are orthogonally arranged. Support beams prevent collapse, maintaining an even 10-μm height over the 2 × 2-mm compression regions of interest. (*c*) Proof-of-concept confocal images show the top view and cross section as cells transhere from an uncoated bottom surface to a top C1-coated surface over 3 h. (*d*) Proteins were striped in parallel lanes in the multiplexed format where eight orthogonally oriented stripes on the top and bottom produce 64 combinations of ECM pairs for testing. C4 corresponds to collagen 4 and Ln to laminin. Surfaces were imaged during compression and after separation. Cells were enumerated on each separated surface to produce heat maps showing percentage of transfer to the top surface for each protein pair. Darker orange indicates proclivity to the top surface whereas darker blue indicates cell preference to adhere to the bottom surface. See Materials and Methods for more details. To see this figure in color, go online.

Bottom surfaces were transferred to a petri dish containing a 1-mm layer of cured PDMS at 40:1 base/cross-linker to prevent motion of the glass piece. Similarly, a 1" × 1" square 40:1 PDMS piece (thickness 2 mm) was placed between the bottom of the top glass substrate and the top compression plate of the platform. Four milliliters of media was added gently over the bottom glass substrate before introducing the top substrate. The top substrate was secured firmly with four nuts and bolts. Cells were allowed to sit sandwiched between the two substrates for 3 h. The four nuts and bolts were unfastened, and the top compression plate was gently lifted and submerged in a new petri dish filled with 5 mL of 1 × PBS.

Pharmacological studies

All pharmacological studies were performed against a control experiment without inhibitor/drug that verified proper functioning of the platform. MDA-lung cells were treated with one of the following: 6.4 μg/mL rabbit anti-α6 integrin (ab84542, lot GR30515; Abcam, Cambridge, United Kingdom), mouse anti-α2 integrin (ab55340; Abcam), rabbit anti-β1 integrin (ab134179; Abcam), 30 μM IPA-3 (I2285; Sigma-Aldrich), 0.1 μM latrunculin B, 1 μM jasplakinolide (sc-202191; Santa Cruz Biotechnology, Dallas, TX), 20 μM nocodazole (M1404; Sigma-Aldrich), 5 μM paclitaxel, 50 μM blebbistatin (B0560; Sigma-Aldrich), 10 nM calyculin A (C5552; Sigma-Aldrich), and 10 μM lysophosphatidic acid (L7260; Sigma-Aldrich). These doses were similar to those used in the literature (26–28). Drugs were incubated for 30 min before compression.

Imaging

All imaging was performed on a Ti fluorescence microscope (Nikon, Melville, NY). The platform was first imaged using large scan stitching to identify all ROIs, and the location of the four corner alignment marks were identified before substrate separation. Substrates were separated and the top compression plate and top substrate were submerged in a new 60-mm-diameter petri dish containing PBS to keep the cells viable. After separation, each substrate was positioned according to the location of the alignment marks and imaged with large scan stitching.

Image processing

A MATLAB script (The MathWorks, Natick, MA) was developed to identify all ROIs and then enumerate cells by Hoechst stain on the bottom and top surfaces of each ROI. Percentage transfer and total cell numbers were calculated for each region.

Immunocytochemistry

Cells were fixed with 4% formaldehyde containing 10 μg/mL Hoechst, 10 mM EDTA, and 5 mM $MgCl_2$ for 15 min at 37°C to cross-link the cells and stain the nuclei. Cells were permeabilized with 0.2% Triton X-100 for 20 min. After two PBS washes, substrates were treated with blocking solution (5% goat serum, 1% BSA, and 0.1% v/v TWEEN 20), followed by primary antibody incubation containing blocking solution with 6.4 μg/mL rabbit anti-α6 integrin (ab84542, lot GR30515; Abcam), mouse anti-α2 integrin (ab55340; Abcam), rabbit anti-β1 integrin (ab134179; Abcam), chicken anti-α-tubulin (ab89984, lot GR82981; Abcam), mouse anti-paxillin (ab32084; Abcam), or mouse anti-E-cadherin (sc-21791; Santa Cruz Biotechnology). Secondary antibody incubation included blocking solution with 1:100 goat anti-chicken AF568, goat anti-rabbit AF568, goat anti-rabbit AF647, goat anti-mouse AF568, or goat anti-mouse AF647. Additionally, single-step antibodies and molecules, including phalloidin-AF488, N-cadherin-AF647, and vimentin-AF647, were used in some experiments. Each incubation was done for 1 h at room temperature, with two blocking solution washes in between. Unless otherwise stated, cells on all surfaces had significantly higher integrin expression from the control group, where no primary antibodies were included. HeLa cells were stained with paxillin on a 2D fibronectin-coated surface as a positive control (data not shown).

Matrix metalloprotease activity

Cells were dosed with an Amplite Universal Fluorimetric matrix metalloprotease (MMP) activity assay (AAT Bioquest, Sunnyvale, CA) at 2% v/v for 5 h. The intensity was measured using a Cytation plate reader (BioTek, Winooski, VT).

Statistical analysis

Two-sample test of proportion was used for the data presented in Fig. 2. A Mann-Whitney-U test was applied for the data presented in Figs. 3 and 4 and Fig. S3. A two-sample *t*-test was performed for the data presented in Figs. S2 and S8.

RESULTS

Transhesion concept and workflow

The fundamental idea is to expose a population of cells to two different surfaces, and then carefully separate those two surfaces and count where cells remain attached. As shown in Fig. 1 *a*, cells are seeded onto a surface coated in ECM protein 1, and are sandwiched in a standard 60-mm petri dish against a top surface coated in ECM protein 2. Each surface is composed of a glass backbone and a thin layer of PDMS (Fig. S1) micropatterned with large 5-μm-deep trenches to safely house the cells under a consistent compression height of 10 μm (Fig. 1 *b*; Fig. S2 *a*), such that cells can engage both surfaces in a uniform manner. Due to differences in a combination of factors that may include integrin densities, spread area, MMP production, migration rate, or integrin binding strength, cells will have higher overall affinity to one ECM-coated surface over another. Upon separation of the surfaces, the region is imaged and the percentages of cells that remained and transferred are quantified.

The assay is simply multiplexed using protein stripes orthogonally arranged between the bottom and top surfaces (Fig. 1 *d*). Cells were subjected to combinatorial pairs of eight different ECM proteins that were coated along the microtrenches in parallel stripes (Materials and Methods). Intensity readouts of fluorophore-conjugated proteins coated on the treated surfaces confirm electrostatic adsorption of the proteins after washing (Fig. S2 *b*). ROIs were identified by the intersections of these stripes (Fig. S2 *c*), and upon surface separation, cells were enumerated in each ROI of the top and bottom surface. The resulting percent transfers to the top surface for each ROI were plotted as heatmaps, where orange indicates high transhesion, and blue indicates low transhesion (see Materials and Methods for more details).

Using the platform, we tested five different breast cell lines. hMECs were used as a benchmark for nontransformed breast cells. We also used the well-studied MDA-MB-231 line, and three tropic MDA-MB-231 lines—TGL/1833

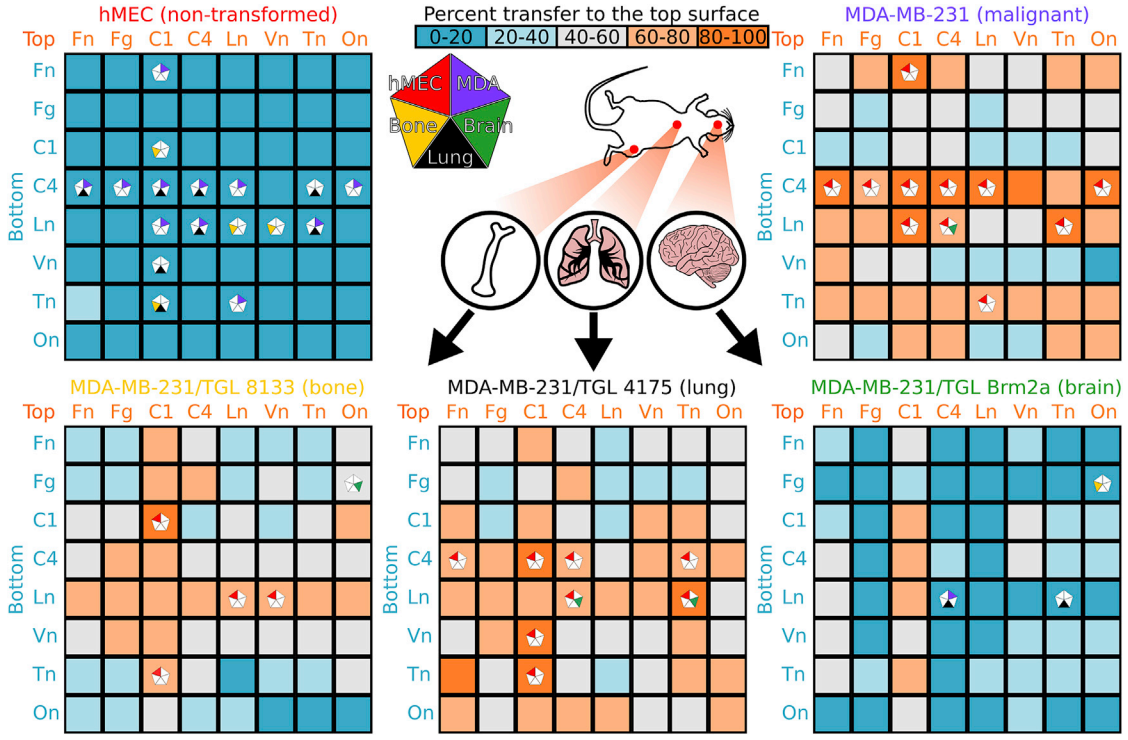

FIGURE 2 Transhesion profiles. Cell transfer is measured and mapped for 64 combinations of protein pairs for five cell lines: hMEC (noncancerous breast epithelial cells), MDA-MB-231 (parent malignant mesenchymal cells), and metastatic MDA cells that are characterized to have tropism to bone, lung, or brain. Darker orange squares indicate a larger percentage of transfer to the top whereas darker blue squares indicate smaller percentage of transfer to the top. For each protein pair and cell line with significant differences in transfer between cell lines, pentagons are shown, with colored wedges indicating p values < 0.01. Shown here are two sample tests of proportion with $n > 800$ cells over six experiments. To see this figure in color, go online.

(bone-tropic), TGL/4175 (lung-tropic), and TGL/Brm-2a (brain-tropic)—as developed by Joan Massagué's lab (4,7,9) and henceforth referred to as "MDA-bone", "MDA-lung", and "MDA-brain", respectively. Fig. 1 *c* shows proof-of-concept confocal cross sections of MDA-lung cells that are fixed between a C1-coated top surface and an uncoated bottom surface at different durations to see the progression of transhesion. All sandwich experiments were performed for 3 h. In a competition between a C1-coated top surface and a Ln-coated bottom surface, we find that MDA-lung cells display a consistent transfer rate to the top when observing cell numbers >100 (Fig. S3 *a*). Similarly, hMEC viability is stable beyond 100 cells per region of interest (Fig. S3 *b*), so we performed all experiments with a minimum of 100 cells. Transhesion is dependent on protein concentration for some ECM proteins (Fig. S3 *c*), but it appears to be uninfluenced by gravitational effects (Fig. S3 *d*). However, for convention, cells are always seeded on the bottom surface and are given the opportunity to transfer to a new top surface.

Mesenchymal phenotypes may promote breast cell transhesion to introduced collagen I surfaces

Using the multiplexed mode, we profiled the five different breast cell lines (Fig. 2) to identify distinct behaviors among those cells. We first notice that viability of MDA-lung cells remaining on either surface after separation was >90%, but only viability of hMEC on their initial Ln-coated surface was >90% (Fig. S3 *e*). Furthermore, C1 had a strong tendency to attract all types of MDA-MB-231 cells to the top surface. Although hMECs are larger than MDA-lung cells on average (Fig. S3 *f*), they do not transfer to the top surface regardless of the presented protein.

Further studies for specific ECM protein pairs and more complex ECM mixtures (Fig. S4) confirm clear differences in transhesion among normal and malignant breast cells, as well as site-specific malignant cells. Both surface ECM proteins and cell type can play a role in cell-environment interactions (Fig. S5).

To help explain these differences in transhesion, we first looked at the morphological features of hMEC and MDA-lung cells remaining on each surface after being subjected to six different combinations of protein pairs: C1 v C4 (collagen IV), C1 v Ln, C4 v C4, C4 v Ln, Ln v C4, and Ln v Ln. A higher spread area and lower circularity usually corresponds to the formation of strong adhesions on a surface that allows for force generation, polarization, and spreading of the cell (29) on a 2D surface. Because hMEC cells tend to be larger than MDA-lung cells, their spread area tends to be slightly larger for most conditions (Fig. 3 *b*). Additionally, hMEC cells typically have high

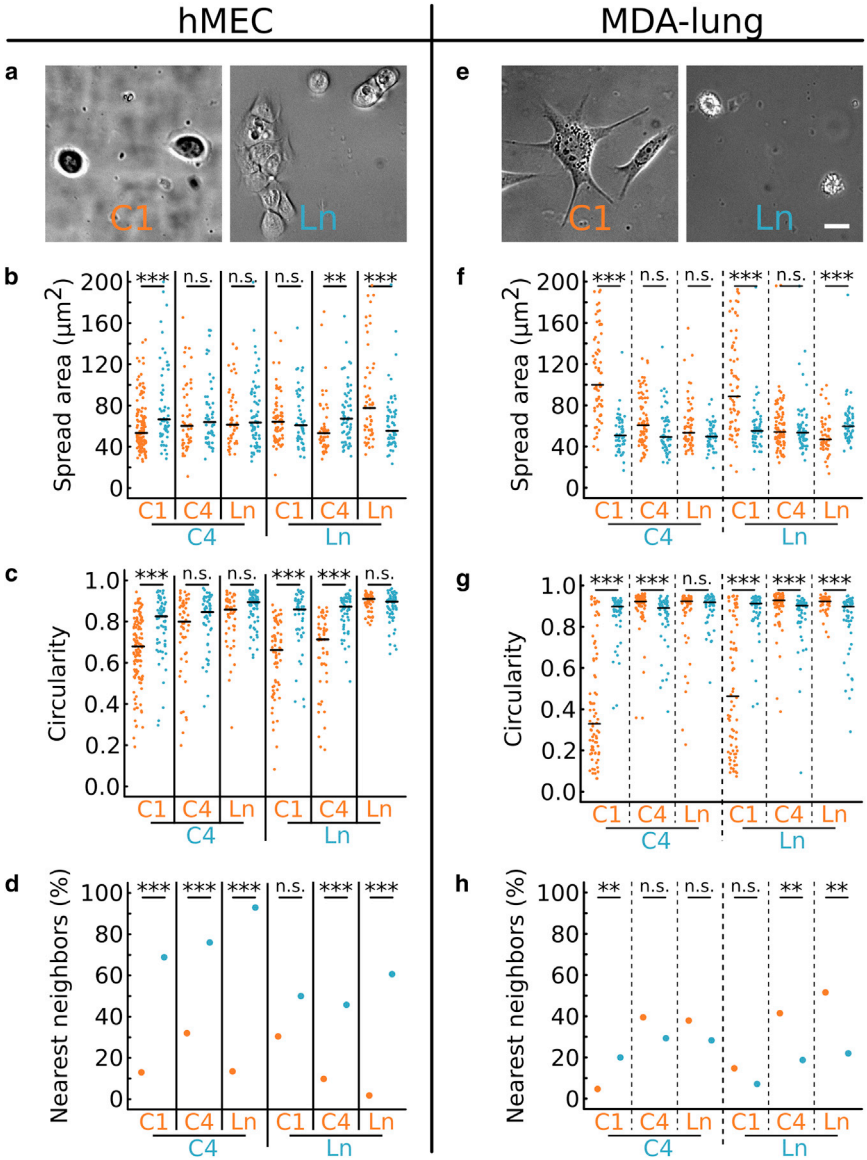

FIGURE 3 Cell morphology of epithelial hMEC and mesenchymal MDA-lung cells for six ECM pair conditions correlated with transhesion. (*a* and *e*) Representative images of cells are spread on a C1-coated top surface and a Ln-coated bottom surface. Scale bars, 10 μm. Cell spread area (*b* and *f*) and circularity (*c* and *g*) measurements highlight MDA-lung cell commitment and polarization on top C1 surfaces in the platform. (*d* and *h*) hMEC remaining on the bottom surface tended to share edges with other cells, indicating stronger preference to form cell-cell adhesions on their initially seeded surface as opposed to transhering. $N \geq 50$ cells. $^{*}p < 0.01$, $^{**}p < 0.005$, and $^{***}p < 0.001$, using Mann-Whitney-U test of medians. To see this figure in color, go online.

circularity (Fig. 3 *c*), which is slightly reduced when they spread on a top C1 surface. Conversely, MDA-lung cells form pseudopodia that increase their spread area (Fig. 3 *f*) and have sharply lower circularity (Fig. 3 *g*) after transhering to the top C1 surface. Despite this, MDA-lung cells do not form focal adhesions on either surface (Fig. S6).

For all conditions, hMEC cells remaining on the bottom surface were significantly more likely to share edges with adjacent cells and appeared to extend short-lived protrusions toward neighboring cells (Fig. 3 *d*; Movie S1), whereas MDA-lung cells spread out without significant cell-cell contact (Fig. 3 *h*; Movie S2). Analysis of vimentin and E-cadherin expression, which are markers of mesenchymal and epithelial phenotypes, respectively, shows pronounced levels of vimentin in MDA-lung cells, and punctate staining of E-cadherin at the edges of hMECs, as expected (Fig. S7). Taken together, general proclivity to C1, combined with mesenchymal-like traits that reduce cell-cell contacts, may correlate with enhanced ability to transfer to C1.

Cell transhesion may be largely dictated by integrin expression and actin assembly

To understand molecular mechanisms contributing to transhesion, we investigated the roles of several cellular components in mediating MDA-lung cell transhesion from one surface to another when subjected to the same six ECM protein pair conditions used in Fig. 3. We first looked into integrins, which are heterodimeric transmembrane proteins that allow cells to interact with ECM directly. In our analysis of integrin binding, we investigated the ubiquitous β1 integrin subunit, as well as α6 and α2 due to their known

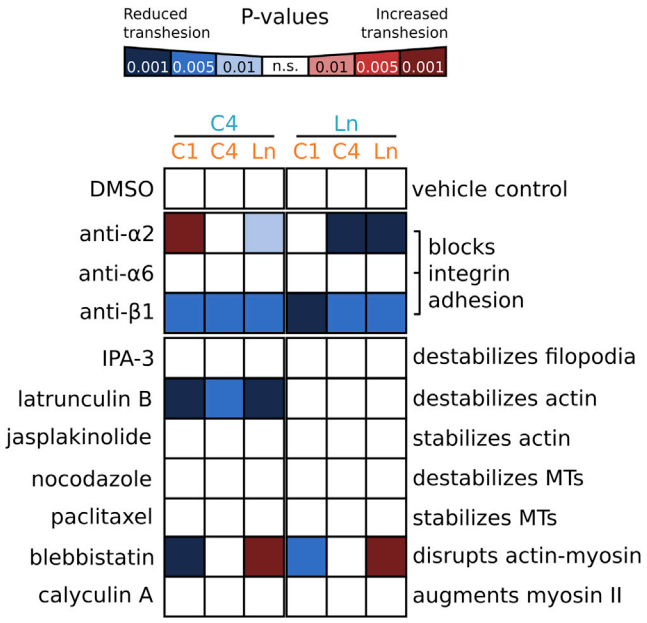

FIGURE 4 Mechanisms of transhesion for MDA-lung cells. Transhesion was observed for cells exposed to six ECM pair conditions and pharmacological and antibody-based inhibition of integrin, filopodia, actin, microtubules (MTs), or myosin. Transhesion knockdown was observed for cells treated with anti-$\alpha 2$ integrin, anti-$\beta 1$ integrin, latrunculin B, and blebbistatin. $n > 3$ for all drug and antibody treatments, and $n > 125$ for MDA-lung control experiments. Mann-Whitney-U test of medians was used for all p values. To see this figure in color, go online.

interactions with laminin and collagens, respectively. Cells were seeded for the normal duration of 2 h, and were then dosed with blocking antibodies to $\alpha 2$, $\alpha 6$, and $\beta 1$ for 30 min. Antibodies to $\alpha 2$ and $\beta 1$ knocked down transfer to the top surface (Fig. 4; Fig. S8), whereas populations treated with $\alpha 6$ antibodies retained the ability to transfer for all protein pairs.

In addition to observing the effects of blocking several integrin components, we found that modulating several intracellular cytoskeletal proteins in MDA-lung cells affected transhesion for several competing ECM-coated surfaces (Fig. 4; Fig. S9). After MDA-lung cells were dosed with latrunculin B, an actin-destabilizing drug, cell transfer was dramatically reduced when cells started on a C4 surface. These MDA-lung cells seemed to display more cell-cell interactions and long pseudopodial protrusions, similar to hMEC (Movie S3). Interestingly, blebbistatin, which disrupts actin-myosin interactions, appeared to knock down transfer to a C1 surface, but increase transfer to a Ln surface. Other drugs we tested that modulate microtubule assembly and breakdown suggest that these processes do not play a dominant role in transhesion.

To test whether degradation of proteins on the bottom surface by cell-secreted enzymes facilitates transhesion to the top surface, we quantified MMP levels in media to reveal a heavy influence of FBS (Fig. S10 *a*). Serum starvation of the cells showed drastic reduction of MMP activity and did cut the transfer rate dramatically (Fig. S10 *b*). This reduction did not recover with addition of lysophosphatidic acid, a component in FBS known to stimulate migration (30). However, due to a multitude of growth factors in FBS, we cannot definitively conclude the role of MMP production as being independent of other factors in FBS on transhesion.

DISCUSSION

Multivariate analyses of phenotypic and genetic biomarkers may provide holistic cellular information that exceeds any single analysis method (31). The transhesion geometry provides integrative measures of a new set of physical biomarkers that show unique differences for malignant cell lines that have varying tropism to metastatic sites in the brain, lung, and bone. Transhesion, to our knowledge, offers a new dimension of analysis that may better resemble cell environments in the human body; these cells are continuously exposed to a multitude of ECM proteins across their surfaces, reflecting the environment of a malignant cell migrating through tissue.

The transhesion platform is readily adaptable for a wide range of studies, and facilitates the parallelization of experiments through the multiplexed setup. For all of our studies, we seeded cells on their initial surface for 2 h, introduced a new surface from above for 3 h, and maintained a uniform gap distance of 10 μm. These parameters are easily tunable for cells of different sizes and adhesion properties. We tested single ECM proteins in each stripe, but more complex, physiologically relevant mixes of ECM proteins can also be tested (Fig. S4 *b*). Cells experience cues from multiple ECM ligands that can uniquely influence the cell. For instance, it has been shown that C1 prevents fibroblasts from stretching Fn by stabilizing the conformation of Fn fibers (32). Interestingly, breast cancer cells can induce surrounding cancer-associated fibroblasts to alter Fn-C1 interactions and promote tumorigenesis (33). Another report suggests that although Fn is highly expressed in breast tumors, Fn promotes proliferation whereas C1 promotes a stretched morphology, spreading, and adhesion (34).

The hMEC line displays epithelial characteristics, where cell-cell adhesions tend to dominate over cell-ECM protein interactions, especially for apical regions of such polarized epithelial cells. Therefore, ECM signals interacting with these cell surfaces after polarization do not effectively promote migration or adhesion. Interestingly, hMECs appear to form bleblike protrusions seemingly as a mechanism of cell-sensing (Movie S1), which resembles amoeboid migration as previously reported in fixed height conditions (35). These protrusions seem to probe the local space for other cells and form cell-cell contacts, which explains the high percentage of nearest neighbors for cells remaining on the bottom surface (Fig. 3).

One of the most striking results is that the malignant cell lines are more likely to transhere, especially if the new

surface is coated in C1. MDA preference to a C1 top surface is supported by our observations of increased spreading, as indicated by larger spread area and lower circularity. This behavior is consistent with histology results, which shows that increased expression and remodeling of C1 corresponds to breast cancer progression (23,36–38). In contrast to hMEC, MDA-MB-231 cells have more mesenchymal features, a phenotype that is associated with increased motility on a 2D surface (39) and in Matrigel (40) as individual cells (41). This may implicate the motile phenotype of mesenchymal cells as a requirement of transhesion, whereas commitment to the top surface is dependent on the ECM protein type, in this case C1.

Despite such spreading, MDA-lung cells were not found to have punctate focal adhesion staining when examined after transhesion to C1. Conversely, hMEC were observed to have nascent focal adhesions on both the top and bottom surfaces. This is in contrast to 2D cultures, where both cell types can show focal adhesion formation after 1 h (Fig. S6). In 2D cultures, seeded cells transition from a suspended state to an adhered state, whereas in our platform, cells start adhered on a surface, but when they transfer they must transition to an adhered state on the new surface before separation. The extended duration of this latter process, as well as having multiple chemical cues of the ECM from opposite surfaces, may delay or prevent focal adhesions from forming in the MDA-lung cells (42).

As with adhesive strength on a 2D surface, the mechanisms contributing to transhesion are complex. However, we discovered several key players that appear critical for MDA-lung cells. Because we selected laminin and the collagens for further study, we chose to observe the effects of inhibition on the integrin subunits most closely associated with adhesion to those ECM proteins: $\alpha 2$, $\alpha 6$, and $\beta 1$. These studies reveal surprising results, such as increased transhesion to C1 despite blocking of $\alpha 2$. This may be due in part to the degree to which antibodies to different integrin subunits block adhesion (43), or whether integrins like $\alpha 2$ largely contribute to initial adhesion as opposed to long-term adhesion (44). Because only dorsal integrins are active to interact with the top surface, integrin blocking may have starkly different effects in this configuration than on 2D surfaces, such as clustering of other integrin types. For further studies, other integrins may be interrogated, such as the vitronectin receptor $\alpha v \beta 3$, which is widely implicated in cancer progression (5,6,45). We also tested numerous drugs that affect other cell components involved in the mechanics of cell adhesion: filopodia, actin, microtubules, and myosin. Of these, it seemed that disruption of the actomyosin complex significantly impaired MDA-lung transhesion. Taken together, transhesion in our platform appears to resemble cell migration in 3D environments, where integrin-ECM binding and actomyosin contractility play important roles (42,46).

When cells were subject to a competition between like proteins (e.g., Fg v Fg) they may transfer at a rate close to 50% given the geometric symmetry, but interestingly, oftentimes cells strongly favor the top surface or the bottom surface due to other unavoidable asymmetries present in the system. For example, strong adhesion of MDA cells to a bottom Vn-coated surface lead to highly spread morphologies, such that cells no longer possessed sufficient height to make contact with the top surface (Fig. S5 *a*). This reduction in transhesion for such cells is also supported by results showing increased $\beta 1$ integrin expression for the small subpopulation of MDA-lung cells that remain very spread out on a Ln-coated bottom surface after the majority of cells transfer to a C1-coated top surface (Fig. S5 *b*). Another factor may be differential degradation of ECM proteins on the initial seeded surfaces, which is largely dependent on the types of MMPs found in the media and expressed by the cells.

Interestingly, when most MDA cell lines are initially seeded on the basement membrane proteins C4 and Ln, they appear to transhere regardless of the protein coated on the opposing top surface. Several sources in the literature suggest multifunctionality in ECM proteins. Malignant breast cells tend to express ADAM-10 and ADAM-17 (47), which can act as both an integrin and a metalloprotease, so they can foster binding and disruption of adhesion (41,43). Antiadhesive effects are seen in several ECM proteins such as thrombospondin (48), tenascin C (49), and laminin (50). Additionally, cells that are seemingly repulsed from the bottom surface may do so because they express MMPs that degrade the proteins patterned on the bottom surfaces. Many malignant cells have also been found to express MMP-2 and MMP-9, which are known to degrade basement membrane proteins like C4 and Ln (51–53). Because cells interact with the bottom surface for 2 h before introduction of the top surface, proteins may have degraded to the point where cells find more adhesive ligands on any new surface. Loss of Ln anchoring has previously been linked to aggressive breast cancer (54) but repulsion to a new surface, as shown in our platform, has not been previously demonstrated. Keeping in mind that integrin-ECM interaction can be characterized by recognition, degradation, and stabilization, transhesion fingerprints can generate more holistic phenotypic information about the cells that cannot be observed with other methods that assay expression levels of integrins alone.

Although previous studies on these site-specific MDA cells have revealed genetic and expression level differences (6–9), this multiplexed tool uniquely characterizes the transhesion of a homogenous cell population, and can later be used as an enrichment platform that enables predictable isolation of subpopulations by the same relative adhesion mechanisms (Fig. S4). Identification of malignant cell populations in tumor biopsies, followed by further delineation of site-specific metastatic proclivity, may

enable early prediction, observation, and treatment of secondary tumors, which are largely responsible for high mortality rates.

Beyond studies of metastatic potential, the transhesion platform can be applied to other cell biology problems, enabled by the design around a standard 60-mm-diameter petri dish. For example, our multiplexed platform can establish differential transhesive fingerprints for induced pluripotent stem cells (iPSCs) and the somatic cells from which they are derived. This may uncover key ECM protein pairs that would allow rare differentiated cells to be extracted from the iPSC culture with the separation platform. By purifying the iPSC culture without bringing them into suspension, we may reduce risks of damage that may be associated with manual processes, enzymatic passaging, or sorting.

SUPPORTING MATERIAL

Ten figures and three movies are available at http://www.biophysj.org/biophysj/supplemental/S0006-3495(17)30921-9.

AUTHOR CONTRIBUTIONS

H.K. designed and performed the experiments and built the platform components. H.K. and D.D. wrote the manuscript. M.Y. provided the cell lines for this study. A.T. designed some of the initial experiments and protocols. A.H. prepared the materials and designed some of the tools used for the study.

ACKNOWLEDGMENTS

We thank Dr. Peter Tseng for discussions during the conception of this project. We thank Michelle Cho for fabricating the materials used for this study. We thank Dr. Oihana Iriondo for providing the cell culture information for this study. We acknowledge the use of the Integrated Systems Nanofabrication Cleanroom at the California NanoSystems Institute at UCLA. The data that support the findings of this study are available from the corresponding author upon request. Computer code used in these studies can be found at https://github.com/hkittur/transhesion.

The work was supported by the National Institutes of Health's (NIH) Director's New Innovator Award No. 1DP2OD007113 and the David and Lucile Packard Fellowship. Confocal laser scanning microscopy (or other appropriate method) was performed at the CNSI Advanced Light Microscopy/Spectroscopy Shared Resource Facility at the University of California, Los Angeles, supported with funding from the NIH-NCRR shared resources grant (CJX1-443835-WS-29646) and National Science Foundation (NSF) Major Research Instrumentation grant (CHE-0722519).

REFERENCES

1. Paget, S. 1889. The distribution of secondary growths in cancer of the breast. *Lancet.* 133:571–573.
2. Togo, S., H. Shimada, …, R. M. Hoffman. 1995. "Seed" to "soil" is a return trip in metastasis. *Anticancer Res.* 15:791–794.
3. Parker, B., and S. Sukumar. 2003. Distant metastasis in breast cancer: molecular mechanisms and therapeutic targets. *Cancer Biol. Ther.* 2:14–21.
4. Kang, Y., P. M. Siegel, …, J. Massagué. 2003. A multigenic program mediating breast cancer metastasis to bone. *Cancer Cell.* 3:537–549.
5. Felding-Habermann, B., T. E. O'Toole, …, B. M. Mueller. 2001. Integrin activation controls metastasis in human breast cancer. *Proc. Natl. Acad. Sci. USA.* 98:1853–1858.
6. Liapis, H., A. Flath, and S. Kitazawa. 1996. Integrin $\alpha v\beta 3$ expression by bone-residing breast cancer metastases. *Diagn. Mol. Pathol.* 5:127–135.
7. Minn, A. J., G. P. Gupta, …, J. Massagué. 2005. Genes that mediate breast cancer metastasis to lung. *Nature.* 436:518–524.
8. Cheng, X., and M.-C. Hung. 2007. Breast cancer brain metastases. *Cancer Metastasis Rev.* 26:635–643.
9. Bos, P. D., X. H. Zhang, …, J. Massagué. 2009. Genes that mediate breast cancer metastasis to the brain. *Nature.* 459:1005–1009.
10. Weigelt, B., J. L. Peterse, and L. J. van 't Veer. 2005. Breast cancer metastasis: markers and models. *Nat. Rev. Cancer.* 5:591–602.
11. Ibrahim, T., I. Leong, …, S. Cheifetz. 2000. Expression of bone sialoprotein and osteopontin in breast cancer bone metastases. *Clin. Exp. Metastasis.* 18:253–260.
12. Oskarsson, T., S. Acharyya, …, J. Massagué. 2011. Breast cancer cells produce tenascin C as a metastatic niche component to colonize the lungs. *Nat. Med.* 17:867–874.
13. Darling, E. M., and D. Di Carlo. 2015. High-throughput assessment of cellular mechanical properties. *Annu. Rev. Biomed. Eng.* 17:35–62.
14. Gossett, D. R., H. T. K. Tse, …, D. Di Carlo. 2012. Hydrodynamic stretching of single cells for large population mechanical phenotyping. *Proc. Natl. Acad. Sci. USA.* 109:7630–7635.
15. Otto, O., P. Rosendahl, …, J. Guck. 2015. Real-time deformability cytometry: on-the-fly cell mechanical phenotyping. *Nat. Methods.* 12:199–202, 4, 202.
16. Hur, S. C., A. J. Mach, and D. Di Carlo. 2011. High-throughput size-based rare cell enrichment using microscale vortices. *Biomicrofluidics.* 5:22206.
17. Koziol-White, C. J., E. J. Yoo, …, R. A. Panettieri, Jr. 2016. Inhibition of PI3K promotes dilation of human small airways in a ρ-kinase-dependent manner. *Br. J. Pharmacol.* 173:2726–2738.
18. Barney, L. E., E. C. Dandley, …, S. R. Peyton. 2015. A cell-ECM screening method to predict breast cancer metastasis. *Integr. Biol.* 7:198–212.
19. Khalili, A. A., and M. R. Ahmad. 2015. A review of cell adhesion studies for biomedical and biological applications. *Int. J. Mol. Sci.* 16:18149–18184.
20. Beningo, K. A., M. Dembo, and Y. L. Wang. 2004. Responses of fibroblasts to anchorage of dorsal extracellular matrix receptors. *Proc. Natl. Acad. Sci. USA.* 101:18024–18029.
21. Fischer, R. S., K. A. Myers, …, C. M. Waterman. 2012. Stiffness-controlled three-dimensional extracellular matrices for high-resolution imaging of cell behavior. *Nat. Protoc.* 7:2056–2066.
22. Rijal, G., and W. Li. 2016. 3D scaffolds in breast cancer research. *Biomaterials.* 81:135–156.
23. DuFort, C. C., M. J. Paszek, and V. M. Weaver. 2011. Balancing forces: architectural control of mechanotransduction. *Nat. Rev. Mol. Cell Biol.* 12:308–319.
24. Singh, A., S. Suri, …, A. J. García. 2013. Adhesion strength-based, label-free isolation of human pluripotent stem cells. *Nat. Methods.* 10:438–444.
25. Pola, C., S. C. Formenti, and R. J. Schneider. 2013. Vitronectin-$\alpha v\beta 3$ integrin engagement directs hypoxia-resistant mTOR activity and sustained protein synthesis linked to invasion by breast cancer cells. *Cancer Res.* 73:4571–4578.
26. Kraning-Rush, C. M., S. P. Carey, …, C. A. Reinhart-King. 2011. The role of the cytoskeleton in cellular force generation in 2D and 3D environments. *Phys. Biol.* 8:015009.
27. Tseng, P., J. W. Judy, and D. Di Carlo. 2012. Magnetic nanoparticle-mediated massively parallel mechanical modulation of single-cell behavior. *Nat. Methods.* 9:1113–1119.

28. Shankar, J., A. Messenberg, …, I. R. Nabi. 2010. Pseudopodial actin dynamics control epithelial-mesenchymal transition in metastatic cancer cells. *Cancer Res.* 70:3780–3790.

29. Iuliano, D. J., S. S. Saavedra, and G. A. Truskey. 1993. Effect of the conformation and orientation of adsorbed fibronectin on endothelial cell spreading and the strength of adhesion. *J. Biomed. Mater. Res.* 27:1103–1113.

30. Du, J., C. Sun, …, X. Lu. 2010. Lysophosphatidic acid induces MDA-MB-231 breast cancer cells migration through activation of PI3K/PAK1/ERK signaling. *PLoS One.* 5:e15940.

31. Lee, W. C., H. Shi, …, K. J. Van Vliet. 2014. Multivariate biophysical markers predictive of mesenchymal stromal cell multipotency. *Proc. Natl. Acad. Sci. USA.* 111:E4409–E4418.

32. Kubow, K. E., R. Vukmirovic, …, V. Vogel. 2015. Mechanical forces regulate the interactions of fibronectin and collagen I in extracellular matrix. *Nat. Commun.* 6:8026.

33. Wang, K., F. Wu, …, D. Gourdon. 2016. Breast cancer cells alter the dynamics of stromal fibronectin-collagen interactions. *Matrix Biol.* 60–61:86–95.

34. Teng, Y., J. Qiu, …, G. Wang. 2014. Effects of type I collagen and fibronectin on regulation of breast cancer cell biological and biomechanical characteristics. *J. Med. Biol. Eng.* 34:62–68.

35. Liu, Y.-J., M. Le Berre, …, M. Piel. 2015. Confinement and low adhesion induce fast amoeboid migration of slow mesenchymal cells. *Cell.* 160:659–672.

36. Levental, K. R., H. Yu, …, V. M. Weaver. 2009. Matrix crosslinking forces tumor progression by enhancing integrin signaling. *Cell.* 139:891–906.

37. Ramaswamy, S., K. N. Ross, …, T. R. Golub. 2003. A molecular signature of metastasis in primary solid tumors. *Nat. Genet.* 33:49–54.

38. Wei, S. C., L. Fattet, …, J. Yang. 2015. Matrix stiffness drives epithelial-mesenchymal transition and tumour metastasis through a TWIST1-G3BP2 mechanotransduction pathway. *Nat. Cell Biol.* 17:678–688.

39. Vuoriluoto, K., H. Haugen, …, J. Ivaska. 2011. Vimentin regulates EMT induction by Slug and oncogenic H-Ras and migration by governing Axl expression in breast cancer. *Oncogene.* 30:1436–1448.

40. Magee, P. J., H. McGlynn, and I. R. Rowland. 2004. Differential effects of isoflavones and lignans on invasiveness of MDA-MB-231 breast cancer cells in vitro. *Cancer Lett.* 208:35–41.

41. Wong, I. Y., S. Javaid, …, D. Irimia. 2014. Collective and individual migration following the epithelial-mesenchymal transition. *Nat. Mater.* 13:1063–1071.

42. Fraley, S. I., Y. Feng, …, D. Wirtz. 2010. A distinctive role for focal adhesion proteins in three-dimensional cell motility. *Nat. Cell Biol.* 12:598–604.

43. Soneral, P., H. Zipoy, and K. Lunacek. 2017. Analysis of cell spreading as a function of integrin inhibition. *FASEB J.* 31:lb165.

44. Carter, W. G., E. A. Wayner, …, P. Kaur. 1990. The role of integrins $\alpha 2\beta 1$ and $\alpha 3\beta 1$ in cell-cell and cell-substrate adhesion of human epidermal cells. *J. Cell Biol.* 110:1387–1404.

45. Sloan, E. K., N. Pouliot, …, R. L. Anderson. 2006. Tumor-specific expression of alphavbeta3 integrin promotes spontaneous metastasis of breast cancer to bone. *Breast Cancer Res.* 8:R20.

46. Petrie, R. J., H. Koo, and K. M. Yamada. 2014. Generation of compartmentalized pressure by a nuclear piston governs cell motility in a 3D matrix. *Science.* 345:1062–1065.

47. Caiazza, F., P. M. McGowan, …, M. J. Duffy. 2015. Targeting ADAM-17 with an inhibitory monoclonal antibody has antitumour effects in triple-negative breast cancer cells. *Br. J. Cancer.* 112:1895–1903.

48. Murphy-Ullrich, J. E., and M. Höök. 1989. Thrombospondin modulates focal adhesions in endothelial cells. *J. Cell Biol.* 109:1309–1319.

49. Husmann, K., S. Carbonetto, and M. Schachner. 1995. Distinct sites on tenascin-C mediate repellent or adhesive interactions with different neuronal cell types. *Cell Adhes. Commun.* 3:293–310.

50. Calof, A. L., and A. D. Lander. 1991. Relationship between neuronal migration and cell-substratum adhesion: laminin and merosin promote olfactory neuronal migration but are anti-adhesive. *J. Cell Biol.* 115:779–794.

51. Jones, J. L., P. Glynn, and R. A. Walker. 1999. Expression of MMP-2 and MMP-9, their inhibitors, and the activator MT1-MMP in primary breast carcinomas. *J. Pathol.* 189:161–168.

52. Gu, Z., J. Cui, …, S. A. Lipton. 2005. A highly specific inhibitor of matrix metalloproteinase-9 rescues laminin from proteolysis and neurons from apoptosis in transient focal cerebral ischemia. *J. Neurosci.* 25:6401–6408.

53. Duffy, M. J., T. M. Maguire, …, N. O'Higgins. 2000. Metalloproteinases: role in breast carcinogenesis, invasion and metastasis. *Breast Cancer Res.* 2:252–257.

54. Akhavan, A., O. L. Griffith, …, J. L. Muschler. 2012. Loss of cell-surface laminin anchoring promotes tumor growth and is associated with poor clinical outcomes. *Cancer Res.* 72:2578–2588.